CHAPTER

5

Nonlinear Potential Flow Models

C.J. Fitzgerald

University of Oxford, Oxfordshire, United Kingdom

5.1 INTRODUCTION AND FUNDAMENTAL PRINCIPLES

5.1.1 Beyond Linear Theory

Primary concerns in early-stage development of wave energy converters (WECs) include proof of concept, feasibility considerations, and design optimization (see summary of standardized path to development given by Koca et al., 2013, based on the report by Ingram et al., 2011). Both numerical and small-scale physical models are utilized at this stage to assess the hydrodynamic performance of the WEC. Incident sea-states are assumed to correspond to 'operational conditions', ie, low steepness regular or (at the design validation stage) irregular waves. Linear frequency-domain and time-domain models provide acceptable levels of accuracy and fast computational times required for design optimization and performance analysis, respectively, in such benign sea states. Until quite recently, many WEC designs have been slow to, or have failed to, progress beyond these early stages of design and development so the deployment of small-scale prototypes in real sea conditions has often not been achieved. Therefore, applications of more accurate nonlinear models (inviscid or viscous) in numerical studies of WEC operation have been and are still quite rare, in particular compared to their widespread use in naval hydrodynamics and offshore engineering.

At present, increasing numbers of WEC designs are reaching the small-scale prototype deployment stage. Thus, survivability and reliability considerations for WEC operation in steeper sea states and more hostile environments are taking higher precedence in WEC design and development. Ongoing expansion of CPU power has meant it is now both desirable and feasible to conduct detailed simulations of wave–body interactions involving large waves using either (inviscid) fully nonlinear potential flow (FNPF) models or (viscous) computational fluid dynamic (CFD) models which solve the Navier–Stokes equations (NSE). In fact, applications of NSE solvers have outpaced those of FNPF models in the field of wave energy, mainly because of the wide availability of commercial and open-source packages eg, OpenFOAM (Weller et al., 1998). Nonetheless, FNPF models provide a computationally efficient method—relative to CFD models—for assessing wave loads and body responses during WEC operation in steep sea states. The origins, fundamental

http://dx.doi.org/10.1016/B978-0-12-803210-7.00005-0

principles, and applications of FNPF models in wave energy are discussed next.

5.1.2 Fundamental Principles

Development of nonlinear models of wave structure interactions was motivated by observations in offshore engineering of the excitation of wave loads and structural responses at frequencies outside those contributing to the linear incident wave energy spectrum. In order to avoid large responses owing to linear excitation, compliant offshore structures, such as tension leg platforms (TLPs), are designed to have natural frequencies above or below the dominant incident wave energy frequencies. However, the high-frequency resonant 'springing' motion of ships and TLPs is a well-known phenomenon which occurs at frequencies above the linear incident range and is excited by second-order sum-frequency forces. Similarly, the slow drift motions of slack moored floating structures, excited by difference-frequency wave forces, occur at frequencies much lower than those present in the ambient spectrum. Neither phenomenon can be accounted for using linear theory and require at least second-order theory to account for quadratic wave–wave and wave–body interactions.

In the classical higher-order analysis of wave–body interactions a perturbation scheme based on the Stokes expansion is adopted. In this scheme the velocity potential, free-surface elevation, pressure, and other hydrodynamic quantities are expressed as perturbation series in wave steepness up to the desired order and the fully nonlinear boundary conditions are Taylor expanded about the corresponding equilibrium boundary surfaces. The perturbation theory analysis is well established for diffraction problems in the frequency domain, particularly at second order (eg, Kim and Yue, 1989; Chau and Eatock Taylor, 1992), where nonlinearities in the problem formulation are confined to the free surface. Malenica and Molin (1995) describe an extension of the approach to third order.

FNPF models of wave–structure interactions in three dimensions have proliferated since the earliest proposed schemes, cf. Romate (1989), Yang and Ertekin (1992), Broeze (1993), and Ferrant (1994), owing to increases in computational resources and advances in computational methods. The fundamental difference between FNPF theory and the higher-order radiation/diffraction models based on perturbation expansions is that the assumption of small wave steepness $\varepsilon \ll 1$ is discarded—formal convergence of the perturbation series is no longer required for FNPF models. Thus, finite displacements of the free-surface and wetted-body surfaces are permitted. In particular, wetted-body surfaces and the free-surface surrounding the bodies within the fluid domain can vary in time so the total fluid domain evolves in time. Boundary conditions are applied on these moving surfaces rather than on the time-invariant quiescent fluid and body boundaries as is the case for higher-order perturbation formulations. Domain boundaries must be tracked in order to apply the boundary conditions at each time step. Such an approach, which leads to the formulation of a new boundary value problem (BVP) at each time step, is far more computationally expensive than the classical perturbation scheme and has, in the past, been overlooked in favour of the higher order perturbation schemes in a design context.

In the FNPF theory, the interactions between marine structures and ocean waves are assumed to occur in the regime where viscous and compressibility effects are negligible, ie, water is assumed to behave as an ideal fluid. The assumption of incompressibility is standard in offshore engineering (due to the low velocities encountered during interactions); however, viscous effects may play a significant role depending on the flow regime, wave amplitudes, and wavelengths relative to the body size. For large structures with relatively small motions, such as

offshore platforms, flow separation is localized around any sharp corners and negligible elsewhere. Therefore, boundary layers are relatively thin and so viscous and drag forces are much smaller than the corresponding potential flow forces. However, floating buoy WECs are generally significantly smaller than offshore platforms and vessels. Furthermore, such floating WECs are expected to undergo large excursions for the purposes of energy extraction. Boundary layer thickness may be nonnegligible relative to body dimensions and flow separation may occur as a result of large device excursion amplitudes. Potential flow forces will continue to be the dominant wave loading in wave energy interactions, giving justification to the ideal fluid assumption. However, the relative size of viscous and nonlinear hydrodynamic forces is not *a priori* known.

Outside floating body boundary layers viscous effects decay to zero and the vorticity remains constant in the absence of boundary layer or flow separation. Therefore, the ideal fluid flow is assumed to remain irrotational throughout the interaction. Based on these assumptions, the NSE can be reduced to the nonlinear potential flow equations by expressing the velocity as the gradient of a scalar potential function. Beyond these standard assumptions of potential flow theory, there are relatively few restrictions on the type of wave–structure interactions that can be modelled. In the presence of a structure, it is necessary to assume the free-surface is a single-valued function of position in the horizontal plane, ie, overturning and breaking waves cannot be modelled. (FNPF models of wave propagation and shoaling in the absence of structures can, in fact, capture overturning or plunging breakers prior to the point where the 'lip' of the wave plunges into the flow beneath (see Longuet-Higgins and Cokelet, 1976, and Grilli et al., 1989, for example).) Wave breaking, wave slamming, and green water events and water exit or entry problems, where turbulence or air entrainment play a role, cannot be modelled by inviscid flow theories.

5.1.3 Applications of FNPF Models in Wave Energy

Reports on FNPF models of the hydrodynamic performance of WECs are relatively scarce in the literature. In a review of nonlinear potential flow and CFD models utilized in WEC performance analysis, Wolgamot and Fitzgerald (2015) sought to compile and examine all available FNPF WEC performance investigations, the most notable of which are briefly discussed next.

Several reports on FNPF modelling of oscillating water column (OWC) devices exist. Clément (1997) presents one of the first investigations into nonlinear hydrodynamic responses for an OWC in two dimensions. Koo and Kim (2010, 2013) describe investigations of the hydrodynamic performance of fixed land-based and floating backward bent duct buoy OWCs also in two dimensions. The underlying FNPF model utilized in both of these OWC studies is described in Koo and Kim (2004) and was developed to solve floating body responses to incident waves in an enclosed domain. The OWC studies required modification of the boundary condition in the OWC chamber to describe free surface interactions with oscillatory compressed air. The coupled dynamics of a submerged cylinder undergoing large motions and the surrounding inviscid fluid, in two dimensions, have been modelled using FNPF theory by Guerber et al. (2010, 2012). The intention of these numerical studies was to develop a tool for modelling a submerged point absorber-type device, eg, CETO (Mann et al., 2007; Caljouw et al., 2011) or the Bristol Cylinder (Davis et al., 1981), by the extension of an existing two-dimensional FNPF numerical representation of a wave tank (see Grilli et al. (1989), Grilli and Subramanya (1996), and related works) for modelling wave generation, propagation, and breaking. Letournel et al. (2014) present a comparative study of a FNPF model with a weak-scatterer approximation, both of which are intended to be utilized in studies of WEC performance. However, a preliminary investigation only of the

motion of a submerged body is reported therein, with wave energy case studies intended as future work.

5.2 FORMULATION OF THE FULLY NONLINEAR POTENTIAL FLOW MODEL

FNPF theory is relatively straightforward to derive and formulate due to the absence of the simplifying approximations typical of the linear theory, eg, linearization of boundary conditions, linear decomposition of the potential, and the assumption of time harmonic motions for the frequency-domain analysis. A derivation of the governing equations and boundary conditions for nonlinear surface wave propagation assuming potential flow conditions can be found in Mei (1983, Chapter 1). Herein, a similar derivation is presented with additional boundary conditions and governing equations to account for the motion of a body in the fluid.

The governing equations of the FNPF theory are derived by applying the assumptions that water is an ideal fluid and that the flow is irrotational. Therefore, the NSE can be simplified to obtain the incompressible Euler equations. In wave–structure interactions in the ocean, a uniform, constant fluid density is typically assumed and so the familiar simplified Euler equations (cf. Lin (2008, Chapter 1) for further discussion) can be derived. The condition for irrotational flow implies that the velocity $\boldsymbol{u}$ can be written as the gradient of a scalar potential ϕ, that is $\boldsymbol{u} = \nabla\phi$. Hereinafter, it is assumed that a Cartesian coordinate system has been adopted so that positions are given by $\boldsymbol{x} = (x, y, z)$ with the z axis pointing vertically upwards and the origin located in the quiescent free surface. Consequently, the governing continuity and momentum equations of potential flow theory can be expressed in terms of the potential ϕ as

$$\nabla^2\phi = 0, \tag{5.1}$$

$$\nabla\left(\frac{\partial\phi}{\partial t} + \frac{1}{2}\nabla\phi\cdot\nabla\phi + \frac{p}{\rho} + gz\right) = 0, \tag{5.2}$$

where p is the pressure in the fluid, ρ is the fluid density, and g is the acceleration due to gravity. These governing equations are simply Laplace's equation and a form of Bernoulli's equation, respectively. A more familiar form of Bernoulli's equation follows after spatial integration (and a simple redefinition of the potential to eliminate any arbitrary integration terms)

$$\frac{\partial\phi}{\partial t} + \frac{1}{2}\nabla\phi\cdot\nabla\phi + \frac{p - p_a}{\rho} + gz = 0, \tag{5.3}$$

where p_a is the ambient or reference pressure on the boundary of the fluid domain.

For the sake of brevity, we consider only floating body WECs with power capture through the translational modes of motion, although floating body WECs absorbing through pitch are not unusual (eg, Gilloteaux et al., 2007). Furthermore, floating OWCs, which extract power from the motion of the air in the chamber through a turbine, have been modelled using FNPF theory as mentioned in Section 5.1.3 but are not considered hereinafter. A typical domain for a two-dimensional open ocean wave–body interaction, assuming constant finite depth, is illustrated in Fig. 5.1. The formulation of the wave–body interaction problem within potential flow theory requires boundary conditions on the free surface and the wetted-body surface in addition to the governing equations for the fluid motion and body motion. The governing equations and boundary conditions (included in Fig. 5.1) are formulated next. When numerically modelling a laboratory wave tank configuration, where the body of fluid is enclosed by solid wall boundaries, normal velocity conditions on the external wall boundaries are also introduced. Such models are referred to as numerical wave tanks (NWTs).

The velocity potential ϕ satisfies Laplace's equation (5.1) throughout the fluid domain $\mathcal{D}(t)$.

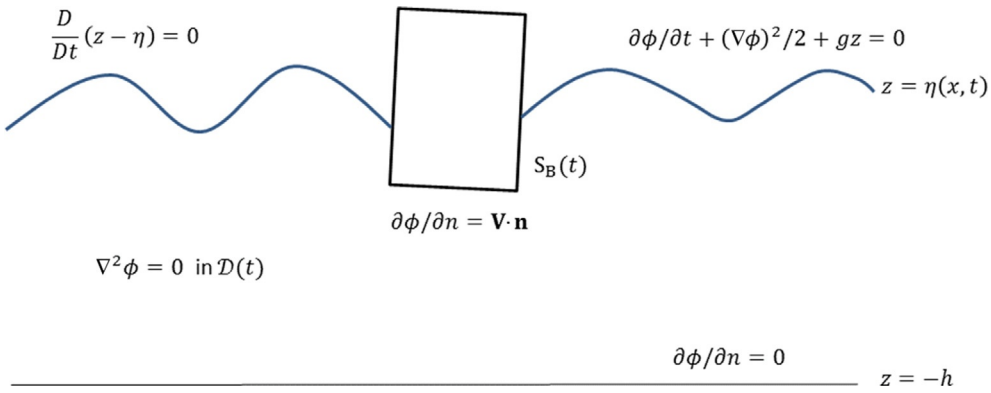

FIG. 5.1 Fluid domain for open ocean wave–structure interaction problem.

Two fully nonlinear conditions hold on the free-surface boundary $S_{\mathcal{F}}$, defined as $z=\eta(x,y,t)$ in three dimensions, which gives the interface between the water and air. No overturning or breaking is permitted so that the free surface is a single-valued function of the horizontal coordinates. The kinematic free-surface boundary condition states that the free-surface $S_{\mathcal{F}}$ must remain intact, that is

$$\frac{D}{Dt}(z-\eta(x,y,t))=0 \quad \text{on} \quad z=\eta, \tag{5.4}$$

where $D/Dt=\partial/\partial t+\nabla\phi\cdot\nabla$ is the convective or Lagrangian derivative. In purely Eulerian terms, the kinematic free-surface condition is given by

$$\frac{\partial\eta}{\partial t}+\frac{\partial\phi}{\partial x}\frac{\partial\eta}{\partial x}+\frac{\partial\phi}{\partial y}\frac{\partial\eta}{\partial y}=\frac{\partial\phi}{\partial z} \quad \text{on} \quad z=\eta(x,y,t). \tag{5.5}$$

Application of Bernoulli's equation on the free-surface where pressure is assumed to equal the ambient (ie, atmospheric) pressure gives the dynamic boundary condition

$$\frac{\partial\phi}{\partial t}+\frac{1}{2}\nabla\phi\cdot\nabla\phi+g\eta=0 \quad \text{on} \quad z=\eta(x,y,t) \tag{5.6}$$

in Eulerian form. The no-flow condition on the sea bed S_{bed}, defined as $z=-h(x,y)$, is given by

$$\frac{\partial\phi}{\partial n}=0 \quad \text{on} \quad S_{bed}, \tag{5.7}$$

where $\frac{\partial}{\partial n}=\boldsymbol{n}\cdot\nabla$ is the normal derivative on the surface with normal vector $\boldsymbol{n}$ directed out of the fluid domain. In deep water, this condition is replaced by the asymptotic condition for the velocity, $|\nabla\phi|\to 0$ as $z\to-\infty$.

With a body present in the fluid domain, a normal velocity condition must also be imposed on the wetted body surface S_{B}, that is

$$\frac{\partial\phi}{\partial n}=V_n \quad \text{on} \quad S_{\mathrm{B}}, \tag{5.8}$$

where $V_n=\boldsymbol{V}\cdot\boldsymbol{n}$ is the component of the body velocity $\boldsymbol{V}$ along the normal to the surface. For a floating body free to respond to incident wave excitation, the governing equations and boundary conditions of the interaction problem must be augmented by the addition of the body's equation of motion. Thus, the body velocity $\boldsymbol{V}(t)$ can, in theory at least, be obtained. For translational motions, the equation of motion is simply given by Newton's second law

$$m\frac{d^2\boldsymbol{X}}{dt^2}=\boldsymbol{F}_{\mathrm{h}}-m\boldsymbol{g}+\boldsymbol{F}_{\mathrm{e}}, \tag{5.9}$$

where $\boldsymbol{X}=(X,Y,Z)$ are the body displacements, m is the body mass, $\boldsymbol{F}_{\mathrm{e}}$ are external forces on the body such as those imposed by moorings, power take-off (PTO) and control mechanisms, $-\boldsymbol{g}=(0,0,-g)$ is the (vector) acceleration due to gravity, and $\boldsymbol{F}_{\mathrm{h}}$

is the force exerted by the fluid on the body. This fluid loading is obtained by integrating the pressure exerted by the surrounding fluid over the wetted body surface

$$\begin{aligned} \boldsymbol{F}_{\mathrm{h}} &= \int_{S_{\mathrm{B}}} p\boldsymbol{n}\, dS, \\ &= -\rho \int_{S_{\mathrm{B}}} \left(\frac{\partial \phi}{\partial t} + \frac{1}{2}\nabla\phi \cdot \nabla\phi + gz \right) \boldsymbol{n}\, dS, \end{aligned} \tag{5.10}$$

where Bernoulli's equation (5.3) has been applied, and comprises (nonlinear) hydrostatic and hydrodynamic components. The coupled nature of the wave–structure interaction problem is clear when one considers the presence of the velocity potential in the hydrodynamic force on the right-hand side of the equation of motion (5.9) and the presence of the body velocity $\boldsymbol{V}$ in the body boundary condition (5.8) for the potential flow problem. The reader is directed to Mei (1983) for a general derivation of the equation of motion of a body free to move in all six modes of motion, and the associated boundary conditions, within the classical perturbation expansion scheme. For wave–body interactions in FNPF theory, more details can be found in Yan and Ma (2007) and Bai and Eatock Taylor (2009) for floating two- and three-dimensional bodies, respectively.

In a domain of infinite horizontal extent we must complement the free-surface and bottom boundary conditions with a finite energy condition

$$\nabla\phi \to 0 \quad \text{as} \quad x^2 + y^2 \to \infty. \tag{5.11}$$

If the domain is bounded, such as for an NWT, then Neumann no-flow boundary conditions on the side walls, and a normal velocity condition on the wavemaker,

$$\frac{\partial \phi}{\partial n} = \boldsymbol{U}_0 \cdot \boldsymbol{n}, \tag{5.12}$$

where $\boldsymbol{U}_0$ is the prescribed wavemaker velocity, will complete the necessary set of boundary conditions. To obtain a fully determined initial BVP, the initial position and velocity of the body and the initial free-surface profile and velocity potential on the free-surface must be prescribed.

Nonlinear terms in the free-surface boundary conditions mean it is impossible to decompose the velocity potential into radiation, diffraction and incident wave components as in the linearized theory. However, the type of problem considered is still classified as a radiation or diffraction problem depending on the body velocity $\boldsymbol{V}(t)$. Therefore, if the body motions are nonzero in otherwise still water, the interaction is classified as a radiation problem, whereas if the body is fixed ($\boldsymbol{V}(t) = 0$ for all t) and subject to incident waves it is a diffraction problem. The problem is classified as a coupled wave-structure interaction problem in the case where the body is floating and free to respond to incident wave excitation. The solution to the coupled wave–body motion problem cannot be reconstructed from the nonlinear radiation and diffraction problems, unlike in the linearized theory, because linear superposition no longer holds and the position of the body and free surface is different in each problem. Nonlinear decompositions for diffracted and incident wave potentials in the diffraction problem do, however, exist (Ducrozet et al., 2014).

The boundaries of the fluid domain, ie, the free-surface, wetted body surfaces, and any enclosing surfaces, vary in time in the absence of linearizing assumptions. Therefore, both the boundary conditions and the boundaries themselves vary in time so that analytical solutions are very difficult (and rare) without some form of approximation (eg, small time expansion). Numerical solutions are necessary and are explored in the next section.

5.3 SOLUTION METHODS FOR FULLY NONLINEAR POTENTIAL FLOW PROBLEMS

An overview of some common numerical solution methods for the problem of a freely floating structure responding to wave excitation in a

bounded domain, governed by the FNPF theory, is provided next. Most solution approaches involve the mixed Eulerian-Lagrangian (MEL) time-stepping scheme and so this is examined in some detail. A brief discussion of the methods used to solve the BVP at the Eulerian stage of the MEL scheme at every time step is also given. High-order spectral (HOS) models of nonlinear wave propagation are also briefly considered.

5.3.1 Mixed Eulerian–Lagrangian Method

Longuet-Higgins and Cokelet (1976) proposed the mixed Eulerian–Lagrangian method to study the evolution of unsteady, nonlinear free-surface waves in two dimensions. Romate (1989), Broeze (1993), and Ferrant (1994) were among the first to generalise the two-dimensional wave–structure interaction implementation of the MEL method to three dimensions. This generalization to three dimensions is conceptually straightforward but in practice quite challenging, particularly around intersections of the floating body and free surface. Nevertheless, the MEL scheme is identical in both two and three dimensions.

The two-stage MEL scheme proceeds as follows at each time step, supposing the boundary of the fluid domain $\partial\mathcal{D}$, the potential ϕ on the free surface boundary, and the normal velocity $\partial\phi/\partial n$ on the body boundary are known at current time t. First, the solution of the potential flow BVP (governing equation (5.1), boundary conditions (5.4)–(5.8), and any domain closure conditions) is determined in the Eulerian frame. In particular, the potential ϕ and normal velocity $\partial\phi/\partial n$ on the wetted body $S_B(t)$ and free surfaces $S_F(t)$, respectively, are obtained. Secondly, the position of the fluid boundaries (including wetted solid boundaries) is advanced in time in the Lagrangian frame by applying the Lagrangian form of the kinematic free-surface boundary condition

$$\frac{D\boldsymbol{x}_F}{Dt} = \nabla\phi, \tag{5.13}$$

where $\boldsymbol{x}_F = (x_F, y_F, y_F)$ is a point on the free surface. An equivalent condition for points on the solid boundaries, including the wetted body surface, is also required where the velocity of the solid boundary replaces the fluid velocity. Furthermore, the boundary data is updated using the dynamic boundary conditions in Lagrangian form. On the free surface, this involves updating the potential using Bernoulli's equation

$$\frac{D\phi}{Dt} - \frac{1}{2}\nabla\phi\cdot\nabla\phi + gz = 0 \quad \text{on} \quad z = \eta, \tag{5.14}$$

whereas on the wetted body surface the normal velocity of the fluid is updated according to the new normal velocity of the body (obtained by integration in time of the body acceleration in the freely floating body case). Explicit time integration of the Lagrangian free-surface boundary conditions (5.13) and (5.14) is only possible because the normal velocity $\partial\phi/\partial n$ has been obtained during the Eulerian solution stage. Similarly, the body velocity can be obtained only if the potential ϕ on the wetted body surface is known thus allowing us to evaluate the pressure force and, using the equation of motion, the acceleration of the body.

In the Eulerian stage of the MEL time-marching scheme, solution of the potential flow BVP is, perhaps, most naturally achieved through the boundary integral equation method (BIEM). This method first requires reformulation of the BVP as a boundary integral equation; Green's second identity is commonly used (eg, Longuet-Higgins and Cokelet, 1976) but Cauchy's integral theorem can also be applied in two dimensions (eg, Dold, 1992). Thereafter, the boundary integral equation is discretized and transformed into a finite system of linear algebraic equations using a boundary element method (BEM). (Indeed, the terms *boundary element method* and *boundary integral equation method* are often used interchangeably.) A detailed examination of a cubic-spline BEM for a fully nonlinear free-surface flow problem in two dimensions is presented by Sen (1995). BEMs are classified according to the order of the polynomials representing the boundary geometry and boundary data (velocity potential and normal velocity) on each discretizing boundary

element; an isoparametric element has geometrical and boundary data representations of equal order. Quadratic isoparametric elements have recently been favoured (cf. eg, Xue et al., 2001; Bai and Eatock Taylor, 2006, 2009) for modelling wave–structure interactions and such higher-order BEMs have largely superseded linear isoparametric methods, eg, Ferrant (1994).

The finite element method (FEM) can be applied as an alternative to the BEM in order to solve the mixed BVP during the Eulerian step of the MEL approach. BEMs have, however, been widely adopted in the past for linear (and second-order) wave–body interactions in the frequency domain because the Green's functions can be chosen so as to satisfy boundary conditions and hence eliminate integration on all but the body surface. In the time domain, a Rankine source Green's function is typically used and integration on the bed only can be eliminated for constant depth problems. Thus, the rationale for using the BEM is weakened. Nevertheless, at first glance it would seem intuitively obvious that a numerical solution method involving discretization of fluid domain boundaries would be more efficient than the corresponding method involving discretization of the entire fluid domain owing to the smaller number of nodes required.

Wu and Eatock Taylor (1995) conducted a comparative study of the FEM and BEM solution methods for a two-dimensional fully nonlinear wave radiation problem and found that the FEM is more efficient, particularly as the number of discretization nodes increases. Both Wu and Eatock Taylor (1995) and Ma et al. (2001a,b) have argued that in terms of CPU and memory the FEM is less demanding than the equivalent BEM. This is due to the properties of the influence coefficients, which contribute to the elements of the system coefficient matrix, and the overall properties of the system matrix. In particular, each band of the FEM matrix will have few nonzero elements (a node is influenced only by contiguous, neighbouring nodes) and the total number of nonzero entries in the coefficient matrix is less than for the equivalent BEM coefficient matrix. Efficient solution methods exist to solve such systems of linear equations involving a sparse coefficient matrix. FEMs were first adopted by Wu and Eatock Taylor (1994, 1995) to solve fully nonlinear free-surface flows and wave–body interactions in two dimensions. Ma et al. (2001a,b) adopted the FEM within the MEL procedure for fully nonlinear interactions between fixed vertical cylinders and waves in three dimensions. Coupled motions of floating bodies and the surrounding fluid have been solved in three dimensions using MEL-FEM, cf. eg, Wu and Hu (2004). More recently, Ma and Yan (2006) developed a new approach, the quasi arbitrary Lagrangian–Eulerian finite element method (QALE-FEM), for simulating fully nonlinear interactions with applications in 2D (Yan and Ma, 2007) and 3D (Ma and Yan, 2009).

5.3.2 High-Order Spectral Methods

HOS schemes have been extensively used to model nonlinear wave propagation and wavefield evolutions on domains representing open sea and wave tank conditions. HOS methods are almost exclusively applied to wave propagation in body-free domains; however, diffraction by a bottom-mounted cylinder has been analysed (Bonnefoy et al., 2006) and hybrid HOS-BEM methods have also been developed. Although HOS methods cannot be truly considered 'fully nonlinear', in the sense that the BEM and FEM implementation of the MEL method can model overturning waves whereas HOS models cannot, high accuracy and fast converging simulations of highly nonlinear wave–wave interactions are achievable. These advantageous properties are a consequence of the underlying spectral basis which facilitates the use of fast Fourier transforms (FFTs) during evaluation. West et al. (1987) and Dommermuth and Yue (1987) developed similar

HOS methods and, as discussed by Schäffer (2008), many subsequent approaches developed independently are in fact equivalent to these original methods.

HOS methods first require the formulation of the nonlinear free-surface boundary conditions in terms of a surface potential (velocity potential evaluated on the free surface $z = \eta$) following Zakharov (1968). The vertical velocity remains the only quantity not explicitly defined on the free surface in the reformulated boundary conditions. The order consistent truncation of these free surface conditions, adopted by West et al. (1987), followed by a pseudospectral expansion yields the solution of the evolution equations from an initial surface potential through the application of FFTs. FFT resolution leads to a computational cost of $O(N\log N)$ at each time step, where $N = N_x N_y$ is the number of grid points discretizing the free-surface. This compares favourably with $O(N^2)$ computational cost for a standard BEM where N is the number of nodes discretizing the domain boundary. (Fast multipole methods are being considered for BEM implementations (Grilli et al., 2010; Harris et al., 2014) which promise to reduce the scaling of computational cost to almost $O(N)$.) Therefore, HOS methods can efficiently model nonlinear wave propagation covering a wide range of length scales on large domains. Dommermuth and Yue (1987) demonstrated how efficient and accurate simulations of nonlinear free-surface flows could be obtained with this method by comparison with simulations from Longuet-Higgins and Cokelet (1976). Further demonstrations are presented by Bonnefoy et al. (2010).

Ducrozet et al. (2006, 2012) extended the order consistent HOS formulation of West et al. (1987), initially developed for open-sea domains, for application to a rectangular NWT. Both wave generation (up to third order in Ducrozet et al., 2012) and wave propagation are modelled using a high accuracy, quickly converging spectral approach referred to as the HOS Tank (HOST) model. HOS Tank has recently been released as an open source code (https://github.com/LHEEA/HOS-NWT/wiki). Coupling with CFD codes is envisaged; HOST wave output could be used to provide input conditions to a CFD wave–structure interaction model. Combination of an efficient inviscid flow solver (such as a HOS method) with a viscous CFD solver to simulate wave motion away from and immediately surrounding the body, respectively, may in due course prove to be the most efficient and accurate method for simulating wave–body interactions and WEC behaviour in steep waves.

5.3.3 Computation of Hydrodynamic Body Forces and Motions

Accurate computation of the hydrodynamic pressure force on a body is crucial to the MEL time-stepping procedure when determining the motion of a freely floating body (and the surrounding free-surface) in steep waves. From Bernoulli's equation (5.3), the pressure comprises the hydrostatic and nonlinear pressure terms $gz + 1/2\,\nabla\phi\cdot\nabla\phi$ and the linear hydrodynamic pressure term ϕ_t. The time derivative of the velocity potential, which is typically the dominant hydrodynamic pressure term, is not automatically obtained during the time-stepping approach. It is critical, therefore, to develop a robust method for computing the time derivative of the velocity potential.

The first, most obvious approach to computing ϕ_t is to apply backward finite differencing. However, many authors, eg, Wu and Eatock Taylor (2003) and Yan and Ma (2007), have noted that this approach suffers from numerical instability, particularly for a floating body problem, and a number of alternative approaches have been proposed. Two approaches, which have proved to be accurate and stable, are based on the idea of obtaining the acceleration potential

ϕ_t or its integral over the body surface as part of the solution of a BVP.

Tanizawa (1995) and van Daalen (1993) formulated a BVP for the acceleration potential ϕ_t, noting that ϕ_t satisfies the Laplace equation, a Dirichlet condition on the free-surface (5.6), a no-flow condition on the fixed solid surfaces and a Neumann condition on the moving body boundary involving translational (and rotational) velocities and accelerations (see Wu (1998) for a full derivation). This BVP cannot be solved in that form due to the presence of the body accelerations on the right hand side of the Neumann body boundary condition, which is unknown before the force has been found. Tanizawa (1995) and van Daalen (1993) sought to eliminate this term by substitution of the equation of motion of the body (5.9), thus giving an implicit body surface boundary condition.

Wu and Eatock Taylor (1996) noted several advantages to this approach but adopted a more indirect solution method upon recognizing that it is the surface integral of ϕ_t rather than ϕ_t itself which is needed. A set of auxiliary functions ψ_i is defined satisfying Laplace's equation on the domain, $\psi_i = 0$ on the free-surface, $\frac{\partial \psi_i}{\partial n} = 0$ on the sea bed, and $\frac{\partial \psi_i}{\partial n} = n_i$ on the body surface for $i = 1,\ldots,3$, where $\boldsymbol{n} = (n_1, n_2, n_3)$ is the unit normal vector on the body surface (positive outwards from the fluid domain). Rotational modes are neglected here but are straightforward to include. Application of Green's second identity to ψ_i and ϕ_t yields an expression for the force integral which can be expressed as

$$F_i = -C_{ij}a_j + q_i, \tag{5.15}$$

where $C_{ij} = \iint_{S_B} \psi_i n_j \, dS$, $a_j = \dot{V}_j$ are the body accelerations, and q_i accounts for the remaining terms with contributions from body velocity and displacement (see Wu and Eatock Taylor (1996, 2003) for full details of the expression for the force integral) and repeated indices imply summation. Crucially, the introduction of the auxiliary potentials allows the calculation of the translational accelerations from

$$(m\delta_{ij} + C_{ij})a_j = q_i - mg\delta_{i3} + (F_e)_i \tag{5.16}$$

for $i = 1,2,3$, prior to the computation of the ith component of the total hydrodynamic force. Through the introduction of the auxiliary potential the mutual dependence of the wave force and body acceleration computations is decoupled. An advantage of both of these methods is that the BVP for ϕ_t or the auxiliary potentials ψ_i is identical in form to that for ϕ and so can be solved simultaneously with little extra computational effort.

Implementations of force computation methods based on the acceleration potential formulation within numerical solutions of fully nonlinear wave–body interaction can be found in the literature for offshore engineering, naval hydrodynamics and more recently wave energy. For example, the implicit boundary condition method of van Daalen and Tanizawa is utilized for the computations of the forces on a floating barge (Koo and Kim, 2004) and later for floating OWCs (Koo and Lee, 2011; Koo and Kim, 2013), in two dimensions. The 'indirect method' involving auxiliary potentials has been implemented in a coupled FEM-BEM NWT (Wu and Eatock Taylor, 2003) and a BEM NWT (Bai and Eatock Taylor, 2006, 2007, 2009), in order to model the response of a submerged floating cylinder and floating vertical circular cylinders, respectively.

5.4 CALCULATING THE WEC RESPONSE

A method for the simultaneous calculation of forces and motions of a body within the MEL time-stepping solution scheme has been outlined in Section 5.3.3. Hereinafter, it is assumed that the wave forces on, and motions of, a floating body can be accurately computed at any time t once the incident wave conditions have

been supplied (eg, through specification of conditions on the outer boundary such as a piston wavemaker displacement signal for a NWT). The floating body is modelled as a WEC by defining the external force term $\boldsymbol{F}_e$ in the equation of motion of the body (5.9) as comprising a PTO and control force, $\boldsymbol{F}_{PTO}$ and $\boldsymbol{F}_C$, respectively. The WEC response in a translational mode of motion is thus obtained from

$$m\frac{d^2\boldsymbol{X}}{dt^2} = \int_{S_B} p\boldsymbol{n}\, dS - m\boldsymbol{g} + \boldsymbol{F}_{PTO} + \boldsymbol{F}_C, \qquad (5.17)$$

where $p = -\rho(\partial\Phi/\partial t + \nabla\phi\cdot\nabla\phi/2 + gz)$ is the nonlinear hydrodynamic and hydrostatic pressure. The vertical component of the buoyancy force $\iint_{S_B} gzn_3\, dS$ counteracts the weight of the body mg and the difference between these forces is simply the hydrostatic restoring force. There are two distinct types of nonlinearity which may occur in the WEC equation of motion. Firstly, the PTO and control terms can be nonlinear with respect to the device motions. Such nonlinear forces can be described within a linear time-domain potential flow solution. Of more importance, however, is the hydrodynamic nonlinearity introduced through the nonlinear pressure term and the time-varying free-surface and body boundary conditions. We try to accurately capture the nonlinear hydrodynamic effects by adopting a FNPF model to describe the wave–body interaction.

Response of the WEC is obtained by solving Eq. (5.17). Bai and Eatock Taylor (2009) achieved this in a straightforward manner within their FNPF implementation by numerical time-integration of Eq. (5.16) for the body accelerations after computation of the wave loads. In a WEC model, the instantaneous power absorption $P(t)$ is obtained from the body motion relative to some reference point as follows

$$P(t) = -\boldsymbol{F}_{PTO}\cdot\dot{\boldsymbol{X}}_{rel}, \qquad (5.18)$$

where the relative body motions are assumed to be constrained to the three translational modes for simplicity. For a single floating buoy WEC the reference point is the seabed and the relative body velocity equals the buoy velocity $\dot{\boldsymbol{X}}_{rel} = \dot{\boldsymbol{X}}$. Two-body WEC systems, often designed for deployment in deep water, achieve power absorption through the relative motion of the bodies and for such WECs the reference point is a floating 'reaction section' which typically has a much larger inertia than the float section.

In the following, we will present the wave loads, body responses, wave run-up, and surrounding free-surface elevations for a single-body floating buoy WEC moving in heave only subject to a linear PTO force.

5.4.1 WEC Response Subject to Linear PTO Forces

A floating body WEC operating in water of uniform depth h is modelled here as a vertical truncated cylinder, constrained to move in heave only, with an associated linear PTO force $F_{PTO} = -\Gamma\dot{Z}$ with a damping coefficient Γ. A simple geometry such as this is unlikely to correspond to a WEC design in practice but it provides a good opportunity for analysing wave loads, body responses and wave run-up on the body for various incident wave conditions. The geometrical specifications (dimensional and dimensionless) for the cylinder and the surrounding water in which it operates are provided in Table 5.1. Mass, length, and time dimensions are rendered dimensionless using the characteristic quantities $(\rho h^3, h, \sqrt{h/g})$. Furthermore, the linear PTO coefficient for the wave absorption simulations is also given in this table—it is chosen to simultaneously allow significant device motions relative to the incident wave amplitude while also achieving reasonable power absorption.

WEC response and power absorption performance in a regular sea state is simulated using the freely floating body form of the fully nonlinear BEM code reported by Bai and Eatock

TABLE 5.1 Properties of Fluid, Fluid Domain, and Truncated Cylinder WEC

Quantity	SI Unit	Dimensionless Value
Water density (ρ)	1025 kg/m^3	1.0
Gravitational accl. (g)	9.807 ms^{-2}	1.0
Water depth (h)	40 m	1.0
Cylinder radius (a)	10 m	0.25
Cylinder draft (d)	20 m	0.50
Displacement volume (V)	6283.19 m^3	0.0981748
Waterplane area (W)	314.159 m^2	0.196350
Mass (m)	6.44027×10^6 kg	0.0981748
PTO coefficient (Γ)	2×10^3 Nm/s	0.0615727

Taylor (2009). Three regular sea states, each of period 7.0 s, with wave amplitudes of 1 cm, 1 m, and 2 m in water of depth 40 m are considered. The corresponding wave steepness parameter kA ranges from $O(10^{-3})$ for the 1 cm wave, to 0.083 and 0.166 for the 1 m and 2 m amplitude waves, respectively. Therefore, the smallest regular wave sea state is effectively linear while the two larger sea states are moderately to strongly nonlinear. To put these steepness values in context, the ratio of wave height to wavelength H/λ for the steepest sea state is 0.0527, corresponding to just over a third of the limiting wave steepness predicted by Stokes. The forces, body motions, wave run-up, and free-surface elevations normalized by the incident wave amplitude are compared next for each sea state to illustrate how nonlinear potential flow effects arise in the free-surface kinematics and body dynamics. However, it is first useful to consider the regime of operation of the cylinder and the spatial and temporal discretization properties for the simulation.

The natural period of oscillation for the cylinder is approximately 10.25 s (found by releasing the body from an initial displacement) and in 7 s incident waves the device is operating far from resonance. The nondimensional body radius parameter ka is equal to 0.83, which implies significant scattering will occur (the weak-scatterer approximation assumes $ka \ll 1$). Mavrakos and McIver (1997) argue that for arrays of interacting bodies, the point-absorber theory based on the weak-scattering approximation is valid for $ka < 0.8$. However, the point-absorber theory assumes optimal motions: for the results presented here the PTO restoring force is zero so that optimal, resonant motion does not occur.

A summary of the dimensions and properties of the computational domain and discretizing mesh, respectively, for the NWT illustrated in Fig. 5.2 is as follows. The domain length L is nine times the depth and the cylinder is located a distance $5.375h$ from the left-hand piston wavemaker boundary, where the depth is assumed to equal unity in the computations. An absorbing sponge layer extends one wavelength from the right-hand side of the tank to absorb the transmitted incident waves and any rightward-travelling scattered waves. Element side-lengths on the free surface far from the body and on the curved cylindrical surface are 0.125 and 0.065, corresponding to 18 and 29 elements per wavelength, respectively. The free-surface element side-lengths gradually increase from the curved cylindrical element length to the far-field free-surface element length. Vertical element lengths immediately below the free surface are approximately 0.035, yielding over 50 elements per wavelength. Nonlinear effects to second-order (at least) should be captured using this relatively fine mesh of quadratic boundary elements. It is worth noting that accurate resolution of higher-order nonlinearities requires large increases in mesh resolution. For example, second-order sum frequency free waves have wavelengths approximately one quarter that of the primary linear component (wavelengths of higher order decrease approximately with the

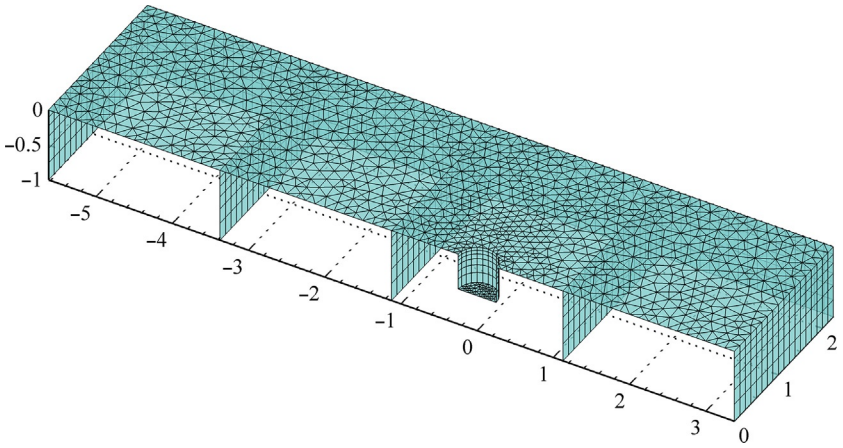

FIG. 5.2 Boundary element discretization of computational domain specified in Table 5.1 including domain decomposition as described by Bai and Eatock Taylor (2007).

square). Element sizes that are small relative to the linear component may be too large to resolve waves at higher orders. Therefore, care must be taken to ensure nonlinearities to the desired order are efficiently and accurately computed for the wide range of length scales involved.

The degrees of nonlinearity in the three incident regular wave fields are illustrated by presenting odd and even harmonic contributions to the free-surface elevation at the proposed location of the cylinder axis, in Fig. 5.3. The fully nonlinear time histories are decomposed into odd and even

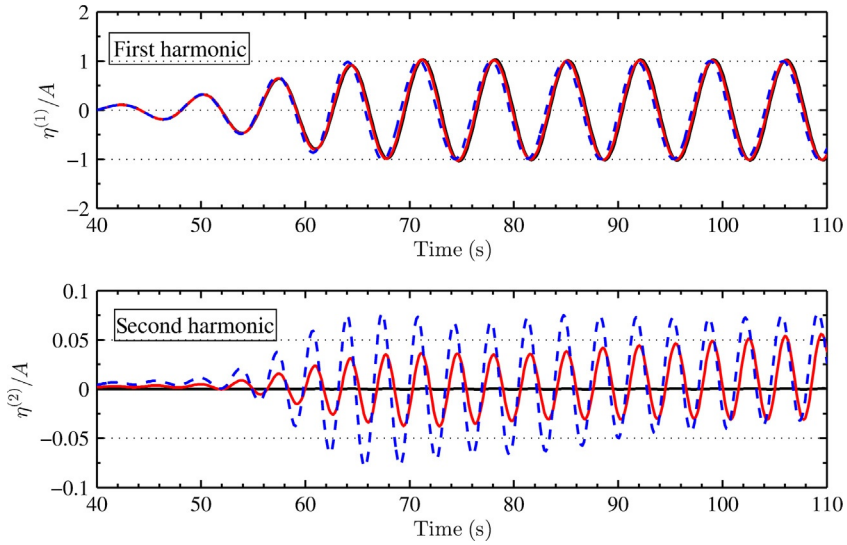

FIG. 5.3 Odd and even harmonics (dominated by first and second harmonics, respectively) per unit wave amplitude of the incident free-surface elevation for waves of amplitude 0.01 m (black), 1.0 m (red; mid grey in print versions), and 2.0 m (blue, dashed; dark grey in print versions).

harmonic components using a phase inversion method described by Borthwick et al. (2006) and Zang et al. (2010), among others, and are dominated by the first and second harmonic contributions in waves of moderate steepness. For the incident free-surface elevations, for example, the odd and even harmonics are effectively the first and second harmonics due to negligible higher order contributions. In order to obtain meaningful comparisons, the elevation and run-up are normalized with respect to the incident wave amplitude. Effects of nonlinearity in the wave kinematics are, as expected, only nonnegligible for the 1 m and 2 m amplitude waves. For the 2 m amplitude waves (steepness coefficient $kA = 0.166$) the second-order component of the free-surface elevation was found to be less than 10% of the linear component.

Time histories of the (normalized) wave run-up at three locations on the circumference of the cylinder are shown for all three incident regular wave amplitudes in Fig. 5.4. The three locations correspond to the upstream face, shoulder and downstream face of the cylinder. Nonlinear effects are most evident at the downstream stagnation point and the odd and even harmonics for the downstream run-up are illustrated in Fig. 5.5 for all three wave amplitudes. Evidence of third harmonic contributions to the odd harmonic of the downstream run-up for the largest incident wave can

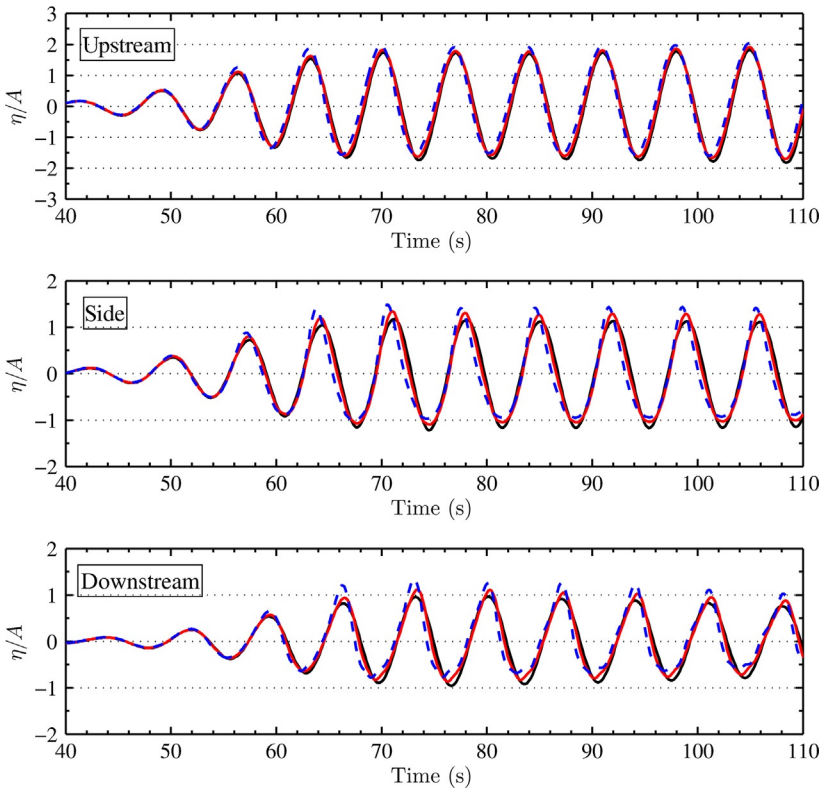

FIG. 5.4 Run-up per unit wave amplitude at the most upstream point of the cylinder, at the shoulder or side of the cylinder and at the most downstream point for incident waves of amplitude 0.01 m (black), 1.0 m (red; mid grey in print versions), and 2.0 m (blue, dashed; dark grey in print versions).

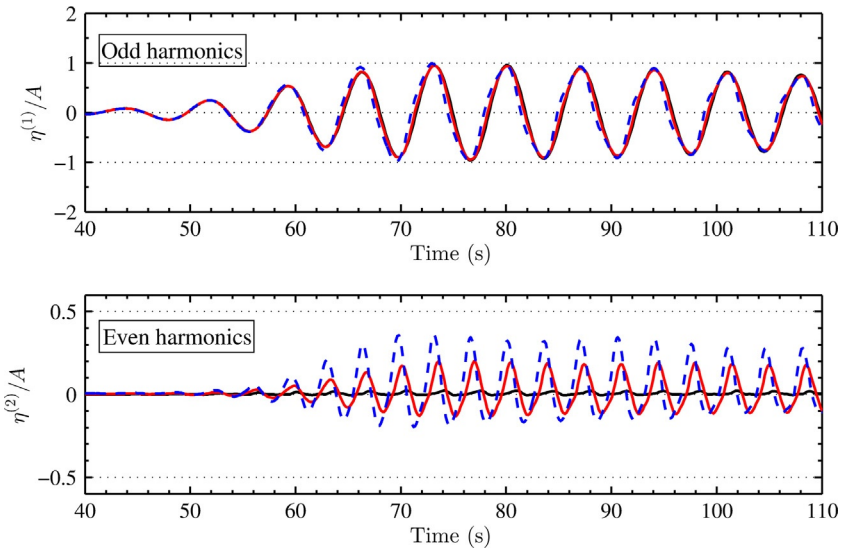

FIG. 5.5 Odd and even harmonics of the wave run-up per unit wave amplitude at the most downstream point of the cylinder for incident waves of amplitude 0.01 m (black), 1.0 m (red; mid grey in print versions), and 2.0 m (blue, dashed; dark grey in print versions).

be observed through the small departures in the shape of the run-up oscillations compared to the sinusoidal shapes for the smaller sea states. The second harmonic of the wave run-up is observed to be approximately 25% of the first harmonic in the steepest waves.

Nonlinear interactions clearly influence the flow kinematics around the cylinder. One source of nonlinearity is the incident wave–wave interactions, which cause higher-order bound waves to propagate along with the linear (free) wave train, as evident in Fig. 5.3. The wave–body interaction, which can enhance free-surface displacements around the body due to diffraction and radiation, also increases nonlinear contributions to the wave kinematics particularly at the intersection line between the cylinder and free surface as evidenced in Fig. 5.5. However, given the typically narrow-banded nature of the response amplitude operator (RAO) curve around resonance for a point absorber, it is worth examining whether such kinematic nonlinearity has a material effect on the body dynamics.

The surge and heave wave loads (per unit wave amplitude) on the heaving cylinder are shown in Fig. 5.6 for each sea state. Apart from a small phase shift, due to the nonlinear dispersion effects which enhance the incident wave celerity, and a small reduction in trough depth, there is little evidence of nonlinear contributions to the surge force. However, the heave force exhibits strong nonlinear effects as the wave amplitude increases. Small but significant departures from the effectively linear time history are observed even for the 1 m incident wave. Decomposition of the heave force into odd and even harmonics is shown in Fig. 5.7. The second-order sum-frequency harmonic (dominating the even harmonic) of the heave force is approximately 25% of the linear harmonic—quite a significant modification to the linear load.

Heave response of the cylinder is illustrated in Fig. 5.8. Before considering any changes in behaviour with increasing wave amplitude, it must first be noted that the response amplitude is approximately one-tenth of the incident wave amplitude. That is, the WEC system is not tuned

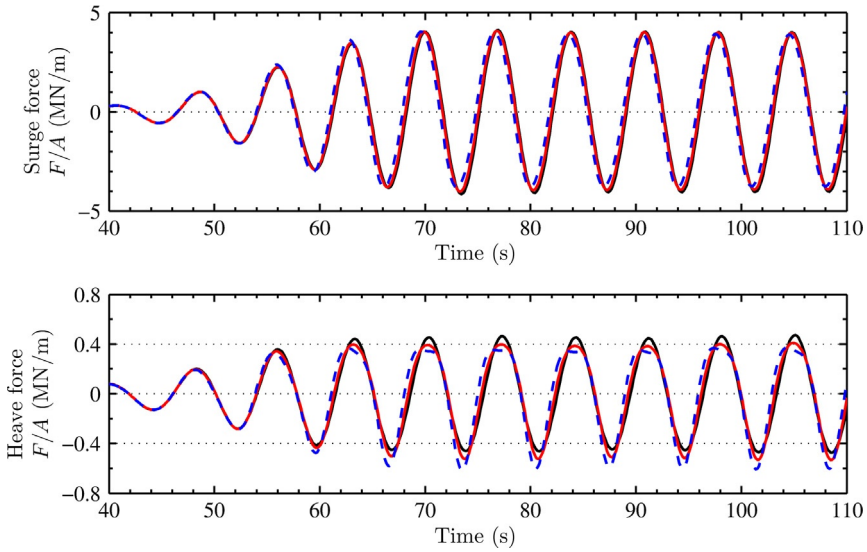

FIG. 5.6 Surge and heave wave loads per unit wave amplitude on the truncated cylinder for incident waves of amplitude 0.01 m (black), 1.0 m (red; mid grey in print versions), and 2.0 m (blue, dashed; dark grey in print versions).

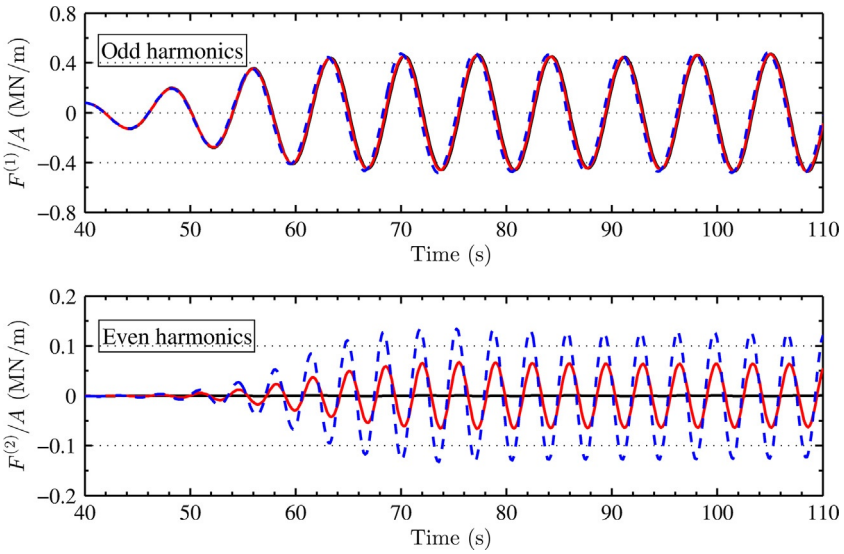

FIG. 5.7 Odd and even harmonics of the heave force per unit wave amplitude on the truncated cylinder for incident wave amplitudes of 0.01 m (black), 1.0 m (red; mid grey in print versions), and 2.0 m (blue, dashed; dark grey in print versions).

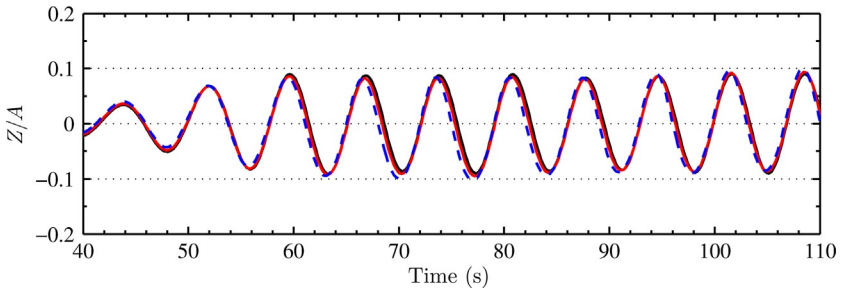

FIG. 5.8 Heave response per unit wave amplitude of the truncated cylinder for incident waves of amplitude 0.01 m (black), 1.0 m (red; mid grey in print versions), and 2.0 m (blue, dashed; dark grey in print versions).

for the incident sea state—the incident wave period is significantly smaller than the WEC resonant frequency. Furthermore, higher order contributions to the device motion appear to be quite small. Instantaneous power absorption from the linear PTO is shown in Fig. 5.9. Increasing the wave amplitude from 1 m to 2 m yields a 5% increase in the normalized mean power capture. That is, nonlinear dynamics contribute to a 5% increase in the power capture relative to the purely linear response. This example is purely illustrative and no general conclusions can be made. However, a more comprehensive investigation into the effects of second-order potential flow hydrodynamics on wave energy performance was conducted by Wolgamot et al. (2015), who analysed a square array of four WECs using a weakly nonlinear (second-order) frequency-domain approach. Therein, it was found that second-order forces and motions lead to negligible additional power for a square array of four deep draught truncated cylinders in deep water. In the most favourable case for second-order contributions (shallow water, closely spaced WECs, weakly optimized array PTO for first-order motions) the mean power due to second-order motions was found to be small outside a near-trapped mode (caused by array interactions) resonant region, where second-order power was approximately 30% of first-order power, even when the second-order forces were relatively large.

5.5 LIMITATIONS

A significant limitation of the potential flow theory is the assumption of negligible viscous and rotational flow effects. For large floating bodies in offshore engineering (floating oil platforms and FPSOs) where the bodies are engineered to minimize motions this assumption may be valid. However, the typical dimensions of wave energy devices are smaller than those of (floating) oil platforms and FPSOs and the devices must undergo large motions to absorb a significant fraction of the available wave energy. Therefore, viscous effects resulting in pressure drag (due to flow separation) and skin friction drag must be taken into account when predicting the motion of the body.

In the results presented in Section 5.4, comparisons with experimental measurements or NSE viscous-flow solver predictions are not provided and the effects of viscosity cannot be assessed. However, both Koo and Kim (2010) and Koo and Kim (2013) validate nonlinear potential flow simulations (in two dimensions) of fixed and floating OWC motions using existing experimental results. During OWC operation, dissipation of the incident wave energy occurs at the chamber entrance due to form drag—vortex shedding is likely to occur—and on the walls of the chamber due to skin friction. Such viscous losses tend to be most significant at resonance when large oscillatory flow

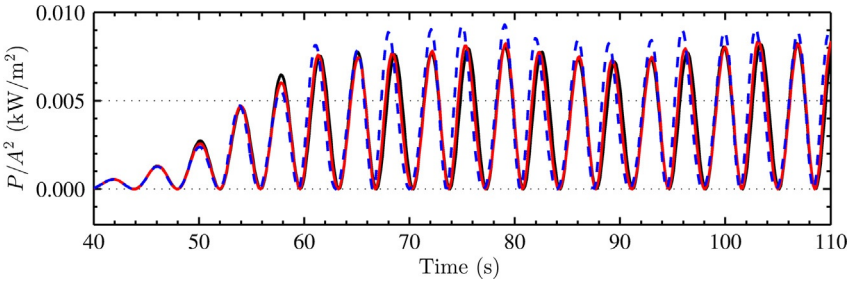

FIG. 5.9 Power absorption per unit wave amplitude squared for incident waves of amplitude 0.01 m (black), 1.0 m (red; mid grey in print versions), and 2.0 m (blue, dashed; dark grey in print versions).

amplitudes occur. Potential flow theory was observed to overestimate the free surface oscillation amplitudes within the chamber by a factor of two at resonance. In order to model the viscous losses within the chamber, the dynamic free-surface boundary conditions in the chamber were modified to include a linear or quadratic viscous damping term. Calibration of the viscous loss coefficient against one experimental test allowed good agreement to be achieved in comparisons with other test results from the same experimental campaign. However, from a design perspective such an approach is not entirely satisfactory—predictions of the operation of a full-scale OWC would require field data to calibrate a new viscous loss coefficient.

Koo and Kim (2013) validated a FNPF model of a floating OWC in operation using physical model laboratory data. In addition to the viscous losses induced by chamber shape, further losses occurred due to the large motions of the OWC. In this case, calibration of two viscous damping coefficients was necessary to achieve good agreement with experimental measurements. Such motion-induced losses are likely to occur for floating buoy devices operating in the point absorber regime also, particularly at resonance when body motions are largest. Nevertheless, viscous drag forces may be approximated using a quadratic Morison-type drag term (see Babarit et al., 2012) and, provided a good estimate of the drag coefficient can be obtained (eg, based on existing empirical results for a body of similar geometry), then the influence of viscosity on body motions may be approximated with reasonable accuracy.

FNPF models have been used to accurately model three-dimensional overturning waves up to the point of plunging (Xue et al., 2001; Grilli et al., 2001). However, when wave–body interactions are modelled, instabilities can arise in the fluid region immediately surrounding the body where diffracted and radiated waves can cause large curvature of the free surface. In the absence of natural damping in the model, unlike CFD solutions of the NSE, instabilities arising during brief periods of large local free-surface deformation tend to persist, even as the large free-surface motions subside, and ultimately lead to the breakdown of the simulation. Instabilities that arise locally can increase in size and scope over time and have a globally destabilizing effect on FNPF simulations owing to lack of dissipation. Artificial damping may be adopted to suppress instabilities and, although these *ad hoc* methods are not always effective, in many cases such transient and local instabilities can be suppressed with local smoothing schemes without affecting the main structure of the flow.

For floating body WECs, it is as yet unclear how important nonlinear potential flow effects are relative to viscous flow effects, particularly at full scale. In offshore engineering, an important design requirement is that the natural resonant frequencies of compliant structures are much higher (or lower) than the dominant incident wave frequencies. However, the high natural frequencies are often lightly damped and if excited can lead to relatively large and persistent oscillations. Fatigue life of the structures can be reduced by such 'springing' or 'ringing' forces. However, the excitation of these structural resonances occurs at harmonics of the incident wave frequency—either due to wave–wave interactions that occur during wave incidence or wave–body interactions. For a floating wave energy device, the primary resonant frequency is designed to occur at the peak of the incident wave energy spectrum. If the device response curve is also narrow-banded around the resonant frequency, then higher harmonics are unlikely to excite significant device responses or play a significant role in device performance. However, broader bandwidth response curves are desirable for WECs so that wave energy can be absorbed over a wider range of incident frequencies. Therefore, higher harmonic excitation may substantially affect the dynamics of such devices. Wave loading on wave energy devices may also be subject to considerable

increases due to higher-order potential flow forces, particularly if the device is restrained from moving, as might be the case in severe sea conditions.

Wave loads occurring during wave breaking, such as slamming loads, and green water events cannot be captured using FNPF models, in contrast to CFD and SPH models. Nonetheless, viscous flow models are often too dissipative to model incident wave propagation accurately whereas FNPF theory can be used to model prebreaking waves with high accuracy. A hybrid FNPF-CFD model wherein wave propagation in an outer domain is modelled using FNPF methods and wave–body interactions in the corresponding inner domain with CFD methods has the potential to harness the advantages of both classes of methods in a wave energy context. Such an approach would not require empirical estimates of Morison-type drag coefficients for a given WEC geometry. To improve the accuracy and widen the applicability of FNPF-only models, a more accurate representation of the drag force on a WEC due to the combined effect of skin friction and flow separation is desirable. Given that the assessment of model success is often with respect to physical models at laboratory scale, it is also important to understand the effects of scaling on the relative importance of viscous and nonlinear potential flow forces.

5.6 SUMMARY

- Wave-body interactions involving steep waves and large device motions (where wave breaking does not occur) can be simulated using FNPF models and so such models are used to evaluate WEC response and WEC loads in extreme sea states.
- FNPF models assume an inviscid, incompressible fluid undergoing irrotational motion and thus are not capable of correctly modelling interactions where viscous effects are significant.
- FNPF models of wave–body interactions typically employ a mixed Eulerian–Lagrangian time-stepping technique, incorporating a BEM or FEM to solve the BVP at each time step, to evolve the motion of the free surface and body in time.
- An example FNPF simulation of a heaving buoy WEC indicates that nonlinear potential flow effects on device response and hydrodynamic loads could be significant.
- FNPF models are less computationally intensive and can model wave propagation with significantly less numerical dissipation and higher accuracy than CFD models. However, lack of natural damping in the model can lead to instabilities where large local wave steepness occurs; artificial damping can be employed to suppress such high-frequency oscillations.
- A coupled FNPF (for wave propagation) with an NSE model (for wave–body interactions) could potentially yield an efficient and accurate nonlinear model without requiring empirical estimates to represent the effect of viscous drag forces on WEC dynamics.

References

Babarit, A., Hals, J., Muliawan, M., Kurniawan, A., Moan, T., Krokstad, J., 2012. Numerical benchmarking study of a selection of wave energy converters. Renew. Energy 41, 44–63.

Bai, W., Eatock Taylor, R., 2006. Higher-order boundary element simulation of fully nonlinear wave radiation by oscillating vertical cylinders. Appl. Ocean Res. 28, 247–265.

Bai, W., Eatock Taylor, R., 2007. Numerical simulation of fully nonlinear regular and focused wave diffraction around a vertical cylinder using domain decomposition. Appl. Ocean Res. 29, 55–71.

Bai, W., Eatock Taylor, R., 2009. Fully nonlinear simulation of wave interaction with fixed and floating flared structures. Ocean Eng. 36, 223–236.

Bonnefoy, F., Eatock Taylor, R., Taylor, P.H., Ferrant, P., 2006. A high-order spectral model for wave interaction with a bottom mounted cylinder. In: Proceedings of the 21st International Workshop on Water Waves and Floating Bodies. Loughborough, UK.

Bonnefoy, F., Ducrozet, G., Le Touzé, D., Ferrant, P., 2010. Time-domain simulation of nonlinear water waves using spectral methods. In: Advances in Numerical Simulation of Nonlinear Water Waves. The World Scientific Publishing Co., Singapore, pp 129–164.

Borthwick, A.G.L., Hunt, A.C., Feng, T., Taylor, P.H., Stansby, P.K., 2006. Flow kinematics of focused wave groups on a plane beach in the UK Coastal Research Facility. Coastal Eng. 53, 1033–1044.

Broeze, J., 1993. Numerical modelling of nonlinear free surface waves with a 3D panel method. Ph.D. thesis, University of Twente, Netherlands.

Caljouw, R., Harrowfield, D., Mann, L., Fievez, J., 2011. Testing and model evaluation of a scale CETO unit. Towards the deployment of a commercial scale CETO Wave Energy Converter. In: Proceedings of the 9th European Wave and Tidal Energy Conference. Southampton, UK.

Chau, F.P., Eatock Taylor, R., 1992. Second-order wave diffraction by a vertical cylinder. J. Fluid Mech. 240, 571–599. http://journals.cambridge.org/article_S0022112092000211.

Clément, A.H., 1997. Dynamic nonlinear response of OWC wave energy devices. Int. J. Offshore Polar Eng. 7(2).

Davis, J., Finney, R., Evans, D., Thomas, G., Askew, W., Shaw, T., 1981. Some hydrodynamic characteristics of the Bristol cylinder. In: Proc. 2nd Int. Sym. Wave Tidal Energ., Cambridge, England, pp. 249–260.

Dold, J., 1992. An efficient surface-integral algorithm applied to unsteady gravity waves. J. Comput. Phys. 103 (1), 90–115. http://www.sciencedirect.com/science/article/pii/002199919290327U.

Dommermuth, D.G., Yue, D.K.P., 1987. A high-order spectral method for the study of nonlinear gravity waves. J. Fluid Mech. 184, 267–288. http://journals.cambridge.org/article_S002211208700288X.

Ducrozet, G., Bonnefoy, F., Le Touzé, D., Ferrant, P., 2006. Implementation and validation of nonlinear wavemaker model in a HOS numerical wave tank. Int. J. Offshore Polar Eng. 16 (3), 161–167.

Ducrozet, G., Bonnefoy, F., Touzé, D.L., Ferrant, P., 2012. A modified high-order spectral method for wavemaker modeling in a numerical wave tank. Eur. J. Mech. B. Fluids 34, 19–34. http://www.sciencedirect.com/science/article/pii/S0997754612000180.

Ducrozet, G., Engsig-Karup, A.P., Bingham, H.B., Ferrant, P., 2014. A non-linear wave decomposition model for efficient wave–structure interaction. Part A: Formulation, validations and analysis. J. Comput. Phys. 257, 863–883. http://www.sciencedirect.com/science/article/pii/S0021999113006220.

Ferrant, P., 1994. Radiation and diffraction of nonlinear waves in three dimensions. In: Seventh International Conference on the Behaviour of Offshore Structures. MIT, USA, pp. 507–524.

Gilloteaux, J.C., Ducrozet, G., Babarit, A., Clément, A.H., 2007. Non-linear model to simulate large amplitude motions: application to wave energy conversion. In: Proceedings of the Twenty-Second International Workshop on Water Waves and Floating Bodies, Plitvice, Croatia, pp. 97–100. http://www.iwwwfb.org/Abstracts/iwwwfb22/iwwwfb22_25.pdf.

Grilli, S., Subramanya, R., 1996. Numerical modeling of wave breaking induced by fixed or moving boundaries. Comput. Mech. 17 (6), 374–391. http://dx.doi.org/10.1007/BF00363981.

Grilli, S., Skourup, J., Svendsen, I., 1989. An efficient boundary element method for nonlinear water waves. Eng. Anal. Boundary Elem. 6 (2), 97–107. http://www.sciencedirect.com/science/article/pii/0955799789900052.

Grilli, S.T., Guyenne, P., Dias, F., 2001. A fully non-linear model for three-dimensional overturning waves over an arbitrary bottom. Int. J. Numer. Methods Fluids 35 (7), 829–867. http://dx.doi.org/10.1002/1097-0363(20010415)35:7⟨829::AID-FLD115⟩3.0.CO;2-2.

Grilli, S.T., Dias, F., Guyenne, P., Fochesato, C., Enet, F., 2010. Progress in fully nonlinear potential flow modelling of 3D extreme waves. In: Ma, Q. (Ed.), Advances in Numerical Simulation of Nonlinear Water Waves. Vol. 11 in Series in Advances in Coastal and Ocean Engineering. World Scientific Publishing Co. Pte. Ltd., Singapore, pp. 75–128 (Chapter 3).

Guerber, E., Benoit, M., Grilli, S.T., Buvat, C., 2010. Numerical modeling of fully nonlinear interactions of ocean waves with a submerged moving body. In: Proceedings of the 3rd International Conference on Ocean Energy, pp. 1–6. Bilbao, Spain.

Guerber, E., Benoit, M., Grilli, S.T., Buvat, C., 2012. A fully nonlinear implicit model for wave interactions with submerged structures in forced or free motion. Eng. Anal. Boundary Elem. 36 (7), 1151–1163. http://www.sciencedirect.com/science/article/pii/S0955799712000288.

Harris, J.C., Dombre, E., Benoit, M., Grilli, S.T., 2014. Fast integral equation methods for fully nonlinear water wave modelling. In: Proceedings of the Twenty-fourth International Offshore and Polar Engineering Conference. International Society of Offshore and Polar Engineers (ISOPE), Busan, Korea, pp. 583–590.

Ingram, D., Smith, G., Bittencourt Ferreira, C., Smith, H., 2011. Protocols for the Equitable Assessment of Marine Energy Converters. The University of Edinburgh, School of Engineering Publishers, Edinburgh, United Kingdom. http://hdl.handle.net/1842/7638.

Kim, M.H., Yue, D.K.P., 1989. The complete second-order diffraction solution for an axisymmetric body. Part 1. Monochromatic incident waves. J. Fluid Mech. 200, 235–264. http://journals.cambridge.org/article_S0022112089000649.

Koca, K., Kortenhaus, A., Oumeraci, H., Zanuttigh, B., Angelelli, E., Cantu, M., Suffredini, R., Franceschi, G., 2013. Recent advances in the development of wave energy converters. In: Proceedings of the Tenth European Wave and Tidal Energy Conference. Aalborg, Denmark.

Koo, W., Kim, M.H., 2004. Freely floating-body simulation by a 2D fully nonlinear numerical wave tank. Ocean Eng. 31, 2011–2046.

Koo, W., Kim, M., 2010. Nonlinear time-domain simulation of a land-based oscillating water column. J. Waterw. Port Coastal Ocean Eng. 136 (5), 276–285. http://dx.doi.org/10.1061/(ASCE)WW.1943-5460.0000051.

Koo, W., Kim, S.J., 2013. Nonlinear time-domain simulation of Backward Bent Duct Buoy (BBDB) floating wave energy converter. In: Proceedings of the Tenth European Wave and Tidal Energy Conference. Aalborg, Denmark.

Koo, W.C., Lee, K.R., 2011. Numerical and experimental analysis of Backward Bent Duct Buoy (BBDB) wave energy converter. In: Proceedings of the Twenty-First International Offshore and Polar Engineering Conference. The International Society of Offshore and Polar Engineers, Hawaii, USA, pp. 655–660.

Letournel, L., Ferrant, P., Babarit, A., Ducrozet, G., Harris, J.C., Benoit, M., Dombre, E., 2014. Comparison of fully nonlinear and weakly nonlinear potential flow solvers for the study of wave energy converters undergoing large amplitude motions. In: Proceedings of the 33rd International Conference on Ocean, Offshore and Arctic Engineering, OMAE 2014, June 8–June 13. San Francisco, California, USA.

Lin, P., 2008. Numerical Modeling of Water Waves. Taylor and Francis, Oxford, England.

Longuet-Higgins, M.S., Cokelet, E.D., 1976. The deformation of steep surface waves on water. I. A numerical method of computation. In: Proceedings of the Royal Society of London A: Mathematical, Physical and Engineering Sciences. 350, pp. 1–26.

Ma, Q., Yan, S., 2006. Quasi ALE finite element method for nonlinear water waves. J. Comput. Phys. 212 (1), 52–72. http://www.sciencedirect.com/science/article/pii/S0021999105003098.

Ma, Q., Yan, S., 2009. QALE-FEM for numerical modelling of non-linear interaction between 3D moored floating bodies and steep waves. Int. J. Numer. Methods Eng. 78 (6), 713–756. http://www.scopus.com/inward/record.url?eid=2-s2.0-65449184488&partnerID=40&md5=e5e9c0dee3e2567fff983c5d9817e946.

Ma, Q.W., Wu, G.X., Eatock Taylor, R., 2001. Finite element simulation of fully non-linear interaction between vertical cylinders and steep waves. Part 1: Methodology and numerical procedure. Int. J. Numer. Methods Fluids 36 (3), 265–285. http://dx.doi.org/10.1002/fld.131.

Ma, Q.W., Wu, G.X., Eatock Taylor, R., 2001. Finite element simulations of fully non-linear interaction between vertical cylinders and steep waves. Part 2: Numerical results and validation. Int. J. Numer. Methods Fluids 36 (3), 287–308. http://dx.doi.org/10.1002/fld.133.

Malenica, Š., Molin, B., 1995. Third-harmonic wave diffraction by a vertical cylinder. J. Fluid Mech. 302, 203–229. http://journals.cambridge.org/article_S0022112095004071.

Mann, L.D., Burns, A.R., Ottaviano, M.E., 2007. CETA, a carbon free wave power energy provider of the future. In: Proceedings of the Seventh European Wave and Tidal Energy Conference. Porto, Portugal.

Mavrakos, S., McIver, P., 1997. Comparison of methods for computing hydrodynamic characteristics of arrays of wave power devices. Appl. Ocean Res. 19 (5–6), 283–291. http://www.sciencedirect.com/science/article/pii/S0141118797000291.

Mei, C.C., 1983. The Applied Dynamics of Ocean Surface Waves. John Wiley and Sons, New York. A Wiley- Interscience Publication.

Romate, J., 1989. The numerical simulation of nonlinear gravity waves in three dimensions using a higher order panel method. Ph.D. thesis, University of Twente, Netherlands.

Schäffer, H.A., 2008. Comparison of Dirichlet–Neumann operator expansions for nonlinear surface gravity waves. Coastal Eng. 55 (4), 288–294. http://www.sciencedirect.com/science/article/pii/S0378383907001275.

Sen, D., 1995. A cubic-spline boundary integral method for two-dimensional free-surface flow problems. Int. J. Numer. Methods Eng. 38, 1809–1830.

Tanizawa, K., 1995. A nonlinear simulation method for 3-D body motions in waves: formulation with the acceleration potential. In: Proceedings of the 10th International Workshop on Water Waves and Floating Bodies. Oxford, United Kingdom.

van Daalen, E., 1993. Numerical and theoretical studies of water waves and floating bodies. Ph.D. thesis, University of Twente.

Weller, H.G., Tabor, G., Jasak, H., Fureby, C., 1998. A tensorial approach to computational continuum mechanics using object-oriented techniques. Comput. Phys. 12 (6), 620–631. http://dx.doi.org/10.1063/1.168744.

West, B.J., Brueckner, K.A., Janda, R.S., Milder, D.M., Milton, R.L., 1987. A new numerical method for surface hydrodynamics. J. Geophys. Res. Oceans 92 (11), 11803–11824. http://dx.doi.org/10.1029/JC092iC11p11803.

Wolgamot, H.A., Fitzgerald, C.J., 2015. Nonlinear hydrodynamic and real fluid effects on wave energy converters. Proc. Inst. Mech. Eng. A: J. Power Energy. http://pia.sagepub.com/content/early/2015/03/24/0957650915570351.abstract.

Wolgamot, H.A., Eatock Taylor, R., Taylor, P.H., 2015. Effects of second-order hydrodynamics on efficiency of a wave energy array. In: Proceedings of the 11th European Wave and Tidal Energy Conference. European Wave and Tidal Energy Conference, Nantes, France.

Wu, G., 1998. Hydrodynamic force on a rigid body during impact with liquid. J. Fluids Struct. 12 (5), 549–559. http://www.sciencedirect.com/science/article/pii/S088997469890158X.

Wu, G., Eatock Taylor, R., 1994. Finite element analysis of two-dimensional non-linear transient water waves. Appl. Ocean Res. 16 (6), 363–372. http://www.sciencedirect.com/science/article/pii/0141118794000298.

Wu, G.X., Eatock Taylor, R., 1995. Time stepping solutions of the two-dimensional nonlinear wave radiation problem. Ocean Eng. 22 (8), 785–798. http://www.sciencedirect.com/science/article/pii/002980189500014C.

Wu, G.X., Eatock Taylor, R., 1996. Transient motion of a floating body in steep water waves. In: Proceedings of the 11th International Workshop on Water Waves and Floating Bodies. Hamburg, Germany.

Wu, G.X., Eatock Taylor, R., 2003. The coupled finite element and boundary element analysis of nonlinear interactions between waves and bodies. Ocean Eng. 30 (3), 387–400. http://www.sciencedirect.com/science/article/pii/S0029801802000379.

Wu, G.X., Hu, Z.Z., 2004. Simulation of nonlinear interactions between waves and floating bodies through a finite-element-based numerical tank. Proc. R. Soc. Lond. A Math. Phys. Eng. Sci. 460 (2050), 2797–2817.

Xue, M., X, H., Liu, Y., Yue, D.K.P., 2001. Computations of fully nonlinear three-dimensional wavebody interactions. Part 1. Dynamics of steep three-dimensional waves. J. Fluid Mech. 438, 11–39. http://journals.cambridge.org/article_S0022112001004396.

Yan, S., Ma, Q., 2007. Numerical simulation of fully nonlinear interaction between steep waves and 2D floating bodies using the QALE-FEM method. J. Comput. Phys. 221 (2), 666–692. http://www.sciencedirect.com/science/article/pii/S0021999106003111.

Yang, C.C., Ertekin, R.C., 1992. Numerical simulation of nonlinear wave diffraction by a vertical cylinder. J. Offshore Mech. Arct. Eng. 114 (1), 36–44.

Zakharov, V., 1968. Stability of periodic waves of finite amplitude on the surface of a deep fluid. J. Appl. Mech. Tech. Phys. 9 (2), 190–194. http://dx.doi.org/10.1007/BF00913182.

Zang, J., Taylor, P.H., Morgan, G., Tello, M., Grice, J., Orszaghova, J., 2010. Experimental study of non-linear wave impact on offshore wind turbine foundations. In: Proceedings of the Third International Conference on the Application of Physical Modelling to Port and Coastal Protection, pp. 1–7.